The Somatostatin-28(1−12)-NPAMAP Sequence: An Essential Helical-Promoting Motif Governing Prosomatostatin Processing at Mono- and Dibasic Sites†

Noureddine Brakch,‡,§ Noureddine Lazar,‡,|| Maï Panchal,|| Flore Allemandou,§ Guy Boileau,⊥ Paul Cohen,|| and Mohamed Rholam*,||

Division d'Hypertension, CHU Vaudois, CH-1011, Lausanne, Switzerland, Université Pierre et Marie Curie, UMR 7631 CNRS, 96, Bd Raspail, 75006 Paris, France, and Département de Biochimie, Université de Montréal, Québec, Case Postale 6128, Montréal H3C 3J7, Canada

Received October 12, 2001

ABSTRACT: Proline residues, known to have special structural properties, induce particular conformations which participate in some biological functions. Two prolines (Pro^{-9}, Pro^{-5}) located near the processing sites (Arg^{-15} and $Arg^{-2}Lys^{-1}$) of human prosomatostatin were previously shown to be important for cleavage of the precursor into somatostatin-28 (S-28) and somatostatin-14 (S-14) [Gomez et al. (1989) *EMBO J. 8*, 2911−2916]. In this study, the importance of the pentapeptide P-A-M-A-P sequence (P-$(X)_3$-P pattern), located in the S-28(1−12) segment connecting the mono- and dibasic cleavage sites, was investigated by using site-directed mutagenesis. Analysis of prosomatostatin-derived peptides produced by expression of mutated cDNA species in Neuro2A cells indicated that (i) deletion of PAMAP decreased S-14 production, (ii) deletion of the two Pro residues almost abolished the cleavage at the dibasic site, and (iii) Pro displacement generating the AMAPP motif resulted in a decrease of S-28 production. Moreover, both theoretical and spectroscopic studies of synthetic peptides reproducing the S-28(1−12) sequence bearing critical mutations showed that this sequence can organize as an α-helical structure. These observations demonstrate that NPAMAP constitutes an accurate α-helix nucleation motif allowing for the generation of equal amounts of S-28 and S-14 from their common precursor in Neuro2A cells. Moreover, they emphasize the importance of the S-28(1−12) segment joining Arg^{-15} and $Arg^{-2}Lys^{-1}$ cleavage sites whose conformational organization is essential for controlling their accessibility to the appropriate processing proteases.

Proteolytic cleavage at monobasic (arginine residue) and dibasic (lysine and arginine arranged in various doublets) sites is the most common processing mechanism to release mature peptide sequences from their larger biosynthetic precursor (*1*, *2*). Only about half of the potential dibasic cleavage sites in prohormones are indeed recognized by their corresponding convertases (*3*). Yeast Kex2 was the first endoprotease unequivocally shown to be involved in prohormone processing. Its functional role was subsequently proven by genetic complementation (*4*). A search of sequence databases led to the discovery of the fur gene encoding a protein called furin and similar to Kex2 (*5*). Several convertases were then discovered (*6*−*9*), and their possible role and tissue distribution were established in relation to their expression in neural, germ, and endocrine cells (*1*, *6*). In addition, several in vitro identified enzymes with dibasic cleavage site specificity have emerged like prohormone thiol protease (*10*), N-arginine dibasic convertase (*11*), and proocytocin/neurophysin convertase (*12*, *13*). Secondary structure motifs such as reverse turns or β-turns were shown to play an essential role to discriminate between functional dibasic residues and those which are not cleaved, generally inserted in organized structures such as β-sheets and α-helices (*3*, *14*−*16*).

Prosomatostatin is a relatively small (=100 amino acid residues) biosynthetic precursor for both somatostatins S-28 and S-14. It undergoes both monobasic (Arg^{-15}) and dibasic ($Arg^{-2}Lys^{-1}$) cleavages to release the two biofunctional hormones (Figure 1A). Production of S-28 and S-14 is both quantitatively and qualitatively variable from tissue to tissue and sometimes from a cell type to another (*17*). This differential tissue-specific processing might be controlled by distinct proteases possibly localized in different subcellular compartments, although they have not been so far unequivocally identified. In mammalian prosomatostatin both mono- and dibasic cleavage motifs occupy the COOH-terminal region of the precursor molecule and are separated by a dodecapeptide segment S-28(1−12), i.e., the NH_2-terminal sequence of S-28. Although no hormonal properties could be conferred to this dodecapeptide, secondary structure predictions underlined the key role that this motif might play in prohormone processing (*17*, *18*). Two β-turns can be positioned respectively upstream and downstream of the $P^{-9}AMAP^{-5}$ pentapeptide motif. Therefore, it can be hypothesized that the 3D organization of this precursor domain

† This work was supported in part by funds from Université Pierre et Marie Curie and the CNRS to UMR 7631.

* To whom correspondence should be addressed. Tel: 33 1 53 63 40 57. Fax: 33 1 42 22 13 98. E-mail:rholam@ccr.jussieu.fr.

‡ These authors contributed equally to this work.

§ Division d'Hypertension, CHU Vaudois.

|| Université Pierre et Marie Curie, UMR 7631 CNRS.

⊥ Département de Biochimie, Université de Montréal.

10.1021/bi011928m CCC: $22.00
Published on Web 01/09/2002

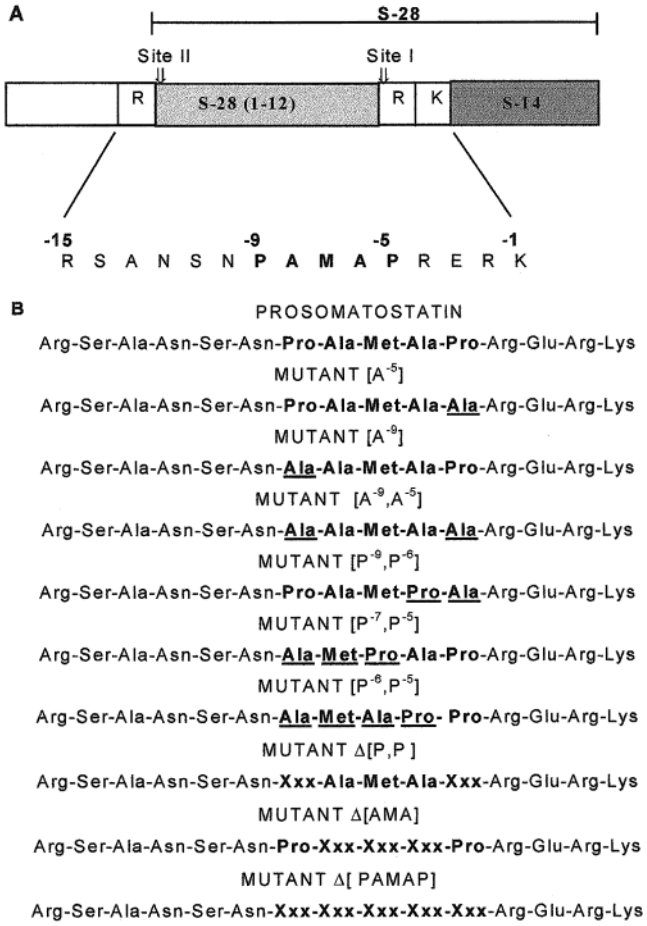

FIGURE 1: Amino acid sequence of the human prosomatostatin region between the monobasic and dibasic cleavage sites. (A) Schematic representation of the human prosomatostatin precursor. Sites I and II correspond to the dibasic (RK) and monobasic (R) cleavage loci for the production of S-14 and S-28, respectively. The S-28(1−12) sequence of S-28 is expanded. (B) Mutated sequences of human prosomatostatin. The substituted residues are underlined.

is appropriate for convertase recognition of the basic amino acid singlet and doublet.

In the present work we have used a combination of the AGADIR predictive method (*19*), of site-directed mutagenesis, and of both circular dichroïsm (CD) and Fourier transform infrared (FTIR) spectroscopies on synthetic peptides reproducing either of the wild-type or relevant mutated prosomatostatin regions to investigate the contribution of the NPAMAP segment to S-28(1−12) conformation. We demonstrate that this peptide sequence is an α-helix promoting motif whose expansion on either the NH_2- or COOH-terminal side, under the control of Pro^{-9} and Pro^{-5}, governs mono- and dibasic proteolytic cleavages.

MATERIALS AND METHODS

Reagents. 2,2,2-Trifluoroethyl alcohol-d_2,OH (99 atom % D) and deuterium oxide (99.97 atom % D) were purchased from Euriso-top (CEA, France).

DNA Manipulations, Construction of Expression Vectors, and Cell Culture. DNA modifications and subcloning, site-directed mutagenesis, and construction of the pN2-Som retroviral expression vectors were performed as described previously (*14*). The presence of mutations in the expression vectors was confirmed by sequencing the mutated regions by the dideoxynucleotide chain-termination method for double-stranded templates using T7 DNA polymerase (*20*).

Infection and Culture Conditions. Preparation of recombinant retroviruses, infections, and a culture of infected Neuro2A cells were performed essentially as described by Noël et al. (*21*). Briefly, viruses were isolated from the culture media of transfected Psi-2 packaging cells and used to infect monolayers of Neuro2A cells for 2.5 h at 37 °C. The viral suspension was then replaced by 5 mL (for 100 mm diameter Petri dishes) of Dulbecco's modified Eagle's medium (DMEM) containing 100 units of penicillin and 200 μg/mL streptomycin sulfate supplemented with 10% fetal bovine serum. Cells were incubated for 48 h before addition of antibiotic G418 at a final concentration of 400 μg/mL.

Analysis of Somatostatin-Related Peptides. Subconfluent infected Neuro2A cells were harvested in phosphate-buffered saline (PBS) (5 mL per Petri dish) with a rubber policeman. A 0.5 volume of glacial acetic acid was added to the cell suspension (*22*). The cell suspension was then sonicated four times for 30 s each. The cell debris was pelleted, and the supernatant was passed through a Sep-Pack C_{18} ODS cartridge (Waters) equilibrated with 0.1% trifluoroacetic acid. The adsorbed peptides were eluted with 40% acetonitrile in 0.1% trifluoroacetic acid. Trifluoroacetic acid and acetonitrile were removed by lyophilization, and the peptides were suspended in 5% acetic acid. The recovery, as determined by control experiments using S-14 and S-28 as standards, was greater than 80%.

Quantification of precursor, S-28, and S-14 molecules in the cell extracts was determined by analyzing cell extracts using a C_{18} reverse-phase HPLC column (Spherisorb ODS15, 250 mm × 4.6 mm) eluted isocratically with 23% acetonitrile and 0.05% trifluoroacetic acid for 40 min and with a gradient of acetonitrile (23−100%) for 25 min at a flow rate of 1 mL/min. Fractions of 1 mL were collected in tubes containing 0.05 mL of glacial acetic acid and were lyophilized. Fractions were assayed for the presence of immunoreactive somatostatin species using a specific radioimmunoassay as described previously (*14*). Control experiments established that for these conditions, with antibodies against S-14 and S-28 exhibited equivalent immunoreactions whereas prosomatostatin was underestimated by a factor of 2. Values were not corrected accordingly.

Peptide Synthesis. Peptides were synthesized using Merrifield solid-phase methodology (*12*) and purified by HPLC using a C_{18} column and a 0−80% linear acetonitrile gradient in 0.1% trifluoroacetic acid. The peptide concentrations were determined through mass estimation and amino acid analysis.

Secondary Structure Predictions. Predictions of secondary structures were performed using the AGADIR algorithm (*19*). This procedure allows calculation of the helicity per residue and the total helicity of peptides, considering short-range interactions in different conditions of solvent, temperature, and pH. The calculated values of those parameters describe the behavior of peptides lacking tertiary interactions in solution.

Circular Dichroism. Circular dichroic (CD) spectra were recorded on a Jobin-Yvon Mark IV linked to a PC microprocessor. Optical cells were placed in a thermostable cell holder. Measurements in the far-UV (190−250 nm) were performed either in H_2O or in H_2O/trifluorethanol mixtures.

Spectra were the average of five consecutive scans recorded at a scan rate of 0.2 nm/s.

Spectra measured were corrected for the buffer baseline and were smoothed. Results are expressed as mean residue ellipticity $[\theta]_R$ (deg·cm^2·dmol^{-1}), which is related to the molar circular dichroism $\Delta\epsilon$ by the following relationship: $[\theta]_R = (3298\Delta\epsilon)/N$, where N is the number of residues. Analysis for prediction of secondary structures from the CD spectra recorded was performed as described elsewhere (*23*).

Fourier Transform Infrared Spectroscopy. Infrared spectra were recorded by means of a Bomem FTIR spectrometer (MB series) linked to a PC microprocessor. The peptides were placed at 25 °C into an infrared cell with CaF_2 plates and a 50 μm path-length spacer. For each spectrum 50 scans were collected at resolution of 4 cm^{-1} and added. During data acquisition, the spectrometer was continuously purged with dry N_2 to eliminate the spectral contribution of atmospheric water. Prior to sample preparation, the trifluoroacetate counterions (TFA)[1] were eliminated as described elsewhere (*24*) in order to eliminate its strong C=O stretching absorption band near 1673 cm^{-1}. Measurements were performed in different mixtures of D_2O/TFE-d_2 for peptide concentrations of 10 mg/mL.

Prior to curve fitting, a straight baseline passing through the ordinates at 1750 and 1500 cm^{-1} was subtracted. Second-derivative spectra accompanied by 5-data-point Savitsky−Golay smoothing were calculated to identify the positions of the components' bands in the spectra (*25*). These wavenumbers were used as initial parameters for curve fitting with Gaussian component peaks. Position, bandwidths, and amplitudes of the peaks were varied until (i) the resulting bands shifted by no more than 2 cm^{-1} from the initial parameters, (ii) all of the peaks had reasonable half-widths (<20−25 cm^{-1}), and (iii) a good agreement between the calculated sum of all components and the experimental spectra was achieved ($r^2 > 0.99$).

The obtained components (amide I band) were assigned to particular structures on the basis of several reports (*25*−*28*), and their relative contents were estimated by dividing the areas of individual peaks by the whole area of the resulting amide I band.

RESULTS

Due to their particular structural properties (*29*) and their multiplicity in certain protein domains, proline residues play a special role in protein structure and function (*30*−*34*). Statistical studies have revealed that, among the P-$(X)_n$-P patterns ($n \leq 5$) analyzed in proteins, the P-$(X)_3$-P motif is the most frequent (*34*). This motif is observed in the peptide S-28(1−12) in which the two proline residues, localized at positions −9 and −5 (see Figure 1A), were shown to be important for processing of the precursor into S-28 and S-14, respectively (*14*, *35*). On the basis of these observations, different mutants of human prosomatostatin cDNA (Figure 1B) were designed in order to evaluate the functional role(s) of the P-$(X)_3$-P motif in the control of cleavage at both the mono- and the dibasic sites.

[1] Abbreviations: D_2O, deuterium oxide; TFA, trifluoroacetic acid; TFE-d_2, 2,2,2-trifluoroethyl alcohol-d_2,OH.

Table 1: Effects of Various Mutations on Human Prosomatostatin Processing in Transfected Neuro2A Cells[a]

mutants	prosomatostatin	S-14	S-28	S-28/S14
wild type	254 (19)	541 (40)	556 (41)	1.0
[A^{-5}]	455 (66)	27 (4)	208 (30)	7.5
[A^{-9}]	206 (44)	238 (51)	20 (4)	0.15
[A^{-9},A^{-5}]	413 (71)	30 (5)	140 (24)	4.8
Δ[P,P]	443 (66)	20 (3)	209 (31)	10
Δ[AMA]	170 (18)	520 (55)	260 (27)	0.5
Δ[PAMAP]	110 (31)	45 (13)	197 (56)	4.4
[P^{-9},P^{-6}]	276 (47)	114 (19)	204 (34)	1.8
[P^{-7},P^{-5}]	2 (4)	228 (40)	313 (56)	1.4
[P^{-6},P^{-5}]	477 (28)	826 (48)	402 (24)	0.5

[a] The amounts of S-28, S-14, and the precursor were evaluated by RIA using antibodies against somatostatin-14. The results are expressed in picograms of S-14 related peptides detected in 5×10^6 cells of mean values from three different experiments (SD = ±15%). Numbers in parentheses represent the fraction of the respective forms as percent of total somatostatin immunoreactivity.

Processing of Prosomatostatin Mutants. Table 1 summarizes the processing efficiencies observed with either the nonmutated precursor or the prosomatostatin mutants. As shown in Table 1, replacement of Pro^{-9} or Pro^{-5} by Ala almost abolished selectively the cleavage of the precursor at the mono- and the dibasic sites. However, the proportions of S-14 ([A^{-9}] mutant) or S-28 ([A^{-5}] mutant) recovered from cell extracts were not similar to that found in the case of the wild type (Table 1) or of mutants in which the basic cleavage sites were mutated selectively (*35*). Moreover, substitution of Ala for both prolines did not impair completely cleavage of mutant [A^{-9},A^{-5}] at the monobasic site (see Table 1). Structural effects induced by substitution of these Pro were investigated by the AGADIR method (*19*). As indicated in Figure 2A, the helicity values per residue of the Som[Arg^{-20}−Asn^{+5}] sequence varied differently when Pro^{-9} and/or Pro^{-5} were (was) replaced by an alanine residue. Indeed, the Pro^{-5} mutation (PAMA**A** motif) induced a more pronounced effect than Pro^{-9} replacement by the same Ala residue (**A**AMAP motif). Furthermore, the helicity values calculated for the Som[Arg^{-20}−Asn^{+5}] sequence bearing the double mutation (**A**AMA**A** motif) were higher than the sum of values obtained for each Pro mutation (Figure 2A). Therefore, selective suppression of cleavage observed in these mutants cannot be related exclusively to local disruption of β-turn structures around each cleavage site (*14*, *15*, *36*) but can be attributed also to global conformational changes.

According to these observations, the effects produced either by deletion of the P-$(X)_3$-P stretch or by modifying its size (Figure 1B) were analyzed in order to evaluate the specific role(s) of each element of this motif in prosomatostatin processing. Results presented in Table 1 underline large differences in the processing of mutants in which the Pro-Ala-Met-Ala-Pro pattern was partially (Δ[AMA] and Δ[PP] mutants) or totally (Δ[PAMAP] mutant) deleted. Indeed, the ratio of S-28 to S-14 produced (S-28/S-14), which was 1 in cells expressing the nonmutated precursor, was reduced to 0.5 for the Δ[AMA] mutant and raised to 4 and 10 for mutants Δ[PAMAP] and Δ[PP], respectively. Moreover, while increase in cleavage at either the monobasic (Δ[PAMAP] mutant) or the dibasic (Δ[AMA] mutant) sites resulted mainly in a decrease in cleavage at the other site, deletion of proline residues induced also a decrease in the processing efficiency of the Δ[PP] mutant (see Table 1). Data

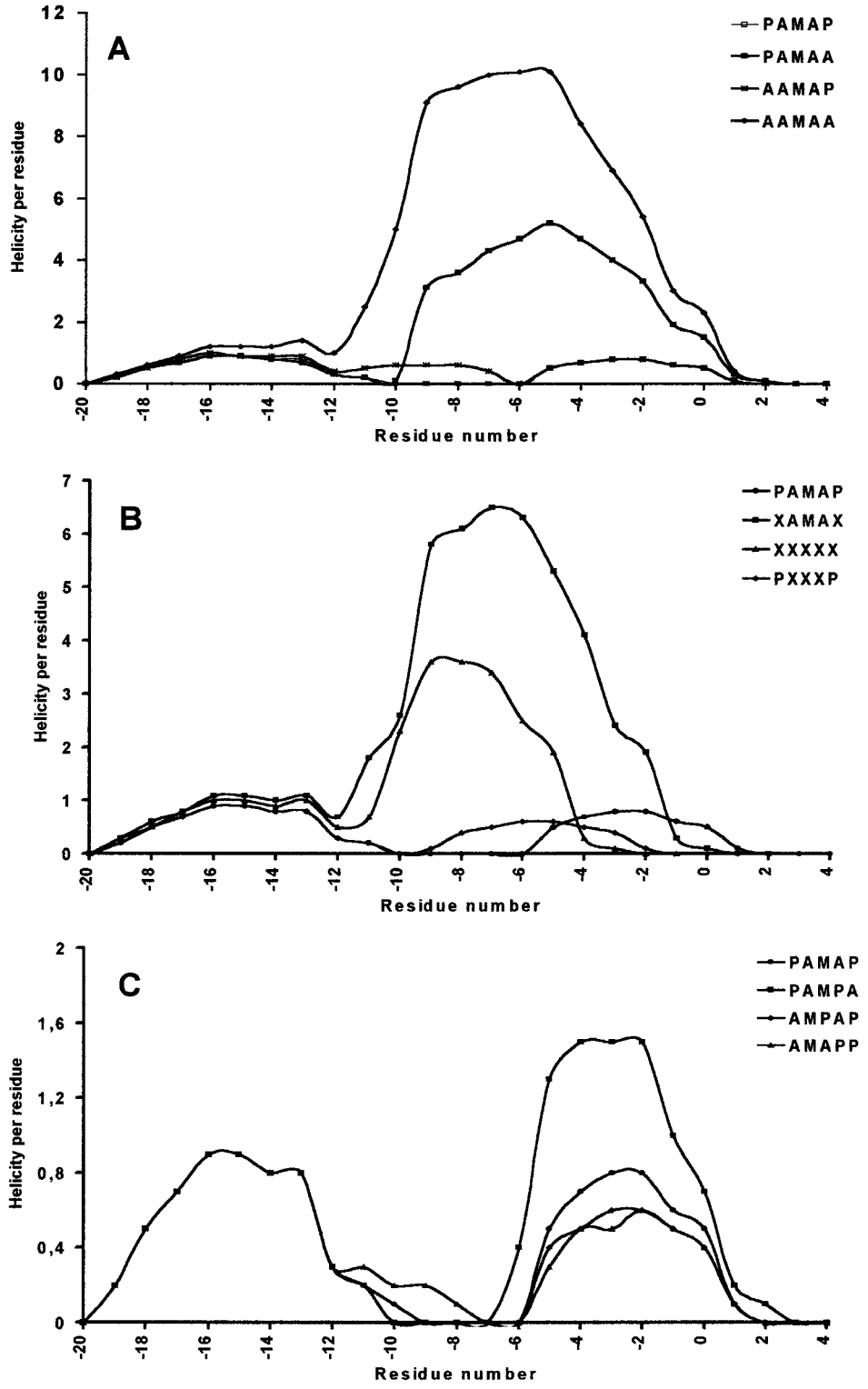

FIGURE 2: Secondary structure prediction of the human prosomatostatin sequence Som(Arg^{-20}—Asn^{-5}). Helicity per residue calculated for peptides in which (A) Pro^{-5} and/or Pro^{-9} were (was) mutated by Ala, (B) the Pro^{-9}-(Xaa)$_3$-Pro^{-5} motif was partially or totally deleted, and (C) the size of the Pro^{-9}-(Xaa)$_3$-Pro^{-5} motif varied.

in Figure 2B indicate that the differences observed in the processing of these mutants were also accompanied by large variations in the helical propensity of the corresponding sequences. Indeed, deletion of the Ala-Met-Ala tripeptide (P**XXX**P motif) decreased exclusively the helicity values per residue of the dibasic site containing domain. In contrast, deletion of either proline residues (**X**AMA**X** motif) or the Pro-Ala-Met-Ala-Pro pattern (**XXXXX** motif) increased both the helicity values and the size of the helical sequence (from 7 to 10 residues). Noticeably these effects were however more pronounced for Pro deletion (Figure 2B). On the basis of these results, comparison of the nonmutated precursor with the Δ[PAMAP], Δ[AMA], and Δ[PP] mutants, respectively, allowed us to deduce the following: (i) the magnitude of cleavage at the dibasic site is under the direct control of the P-(X)$_3$-P motif, (ii) the proline residues positioned upstream

Table 2: Amino Acid Sequences of Som(Arg^{-15}—Lys^{-1})-Related Peptide Substrates[a]

peptide	sequence
Som(Arg^{-15}—Lys^{-1})-PAMAP	Ac-RSANSN-PAMAP-RERK-$CONH_2$
Som(Arg^{-15}—Lys^{-1})-PAMAA	Ac-RSANSN-PAMA<u>A</u>-RERK-$CONH_2$
Som(Arg^{-15}—Lys^{-1})-AAMAP	Ac-RSANSN-<u>A</u>AMA<u>P</u>-RERK-$CONH_2$

[a] Amino acids corresponding to modifications of the original sequence are underlined.

of this cleavage site are essential for the production of higher proportions of the S-14 molecule, and (iii) the Ala-Met-Ala tripeptide appears to be involved in the correct folding of the S-28(1−12) domain.

These conclusions were supported by the results obtained for the processing of prosomatostatin mutants in which the size of the P-$(X)_3$-P motif varied (Figure 1B, Table 1). Analysis of data in Table 1 indicates that the S-28/S-14 ratio increases for the [P^{-9},P^{-6}] and [P^{-7},P^{-5}] mutants whereas it decreases for the [P^{-6},P^{-5}] mutant. Furthermore, the yield of uncleaved precursor recovered from cell extracts for mutants [P^{-9},P^{-6}] and [P^{-7},P^{-5}] (47% and 4%, respectively) was not similar to that found in the case of the wild type (22%) or of the [P^{-6},P^{-5}] mutant (28%). As shown in Figure 2C, the shift of either Pro^{-9} or Pro^{-5} induced essentially variations in the helicity values of the [Met^{-7}−Ala^{+1}] fragment which contains the dibasic cleavage site. Indeed, when compared to the native sequence (**P**AMA**P** motif), the shift of Pro^{-9} to positions −7 (AM**P**A**P** motif) or −6 (AMA**PP** motif) reduced the helicity values per residue of peptides whereas the shift of Pro^{-5} to position −6 (**P**AM**P**A motif) increased these values (Figure 2C). Interestingly, it can be observed that either deletion of the Ala-Met-Ala tripeptide (Δ[AMA] mutant) or shift of the Pro^{-9} residue ([P^{-6},P^{-5}] mutant) decreased the values of both the S-28/S-14 ratio and the helicity per residues whereas deletion of both proline residues (Δ[PP] mutant) or shift of the Pro^{-5} residue ([P^{-9},P^{-6}] mutant) increased these values. This emphasizes the structural role of the Pro^{-9}-Ala-Met-Ala-Pro^{-5} pattern which is constituted by the following: (i) the helical-promoting tripeptide Ala^{-8}-Met-Ala^{-6}, (ii) the Pro^{-9} residue which amplified the helicity of this tripeptide, and (iii) the Pro^{-5} residue which, in addition to its participation to β-turn structure (*36*), stopped the propagation of this small helix-promoting signal on its N-terminal side.

Conformational Analysis of Modified Som(Arg^{-15}—Lys^{-1}) Peptides. To provide structural support for these in vivo and predictive data, peptides corresponding to different sequences were synthesized (Table 2) and then analyzed by CD and FTIR spectroscopy at low TFE concentrations.

CD Analysis. The far-ultraviolet CD spectra of all Som(Arg^{-15}—Lys^{-1}) analogues recorded in aqueous solution, pH 7.0, 25 °C (Figure 3A), displayed a weak minimum at 222 nm (α-helices) and another one between 195 and 200 nm (unordered structures) which was intense for peptide Som[Arg^{-20}—Lys^{-1}]-PAMAP. Addition of 50% TFE strongly modified the profile of those CD spectra (Figure 3B): the intensity of the band between 195 and 200 nm decreased and its maximum was red shifted in particular for Som[Arg^{-20}—Lys^{-1}]-PAMAA and Som[Arg^{-20}—Lys^{-1}]-AAMAP peptides. Such observation reflects the stabilization of ordered structures over the random coil structures (*23*). Indeed, both

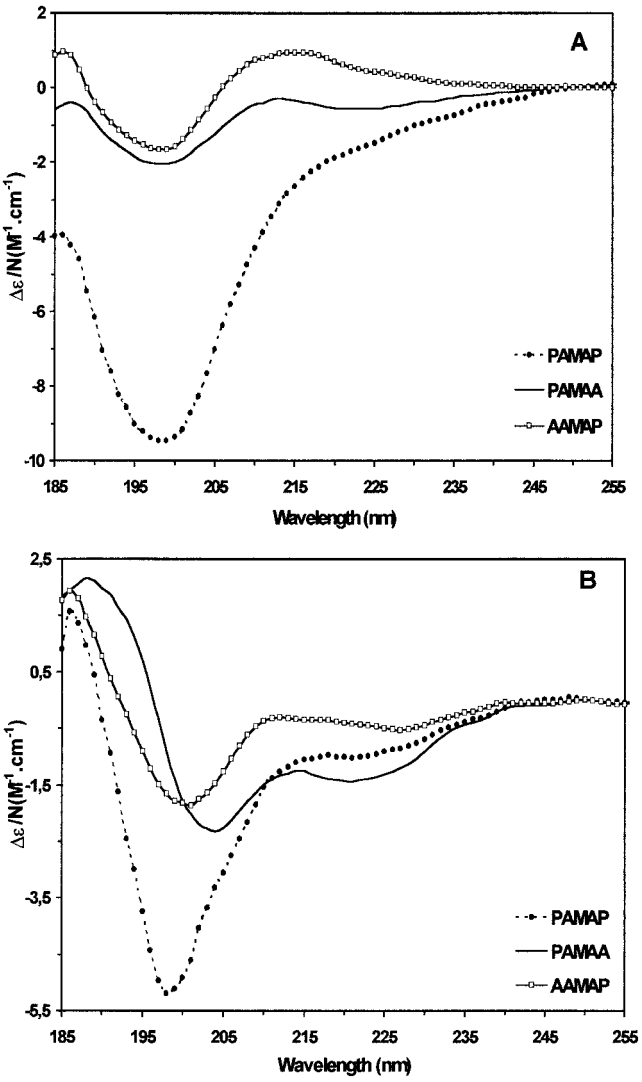

FIGURE 3: CD spectra of human prosomatostatin peptide analogues. Far-UV CD spectra of peptides in H_2O (A) and 50% TFE (B) are shown as mean molar residue ellipticity ($\Delta\epsilon/N$) versus wavelength (nm). Measurements were performed at 25 °C for a 40 μM concentration of peptides.

spectra of the latter peptides showed two minima at 222 nm (helical n → p* transition) and between 202 and 208 (overlapping helical and random coil π → p* transition at 208 and 200 nm, respectively) and a maximum around 190 nm.

The estimation of secondary structures of those Som(Arg^{-15}—Lys^{-1}) peptides from their CD spectra recorded in 50% TFE/H_2O was performed by using different methods (*23*). The deduced intrinsic values varied from one evaluation method to another. But, in all cases, this variation observed between each peptide was always similar in trend and direction. For example, the percentage of α-helix obtained by the Fasman method (*23*) was 27%, 44%, and 37% for peptides Som[Arg^{-20}—Lys^{-1}]-PAMAP, Som[Arg^{-20}—Lys^{-1}]-PAMAA, and Som[Arg^{-20}—Lys^{-1}]-AAMAP, respectively.

FTIR Analysis. Figure 4 shows the infrared spectra of Som(Arg^{-15}—Lys^{-1}) peptides (50% TFE-d_2/D_2O) obtained in the 1700−1500 cm^{-1} region (amide I and II bands) and also the component spectral bands that are used to fit the spectrum of each peptide. For the analysis of the privileged secondary structures adopted by these peptides, only the more informative amide I band was analyzed (*25*).

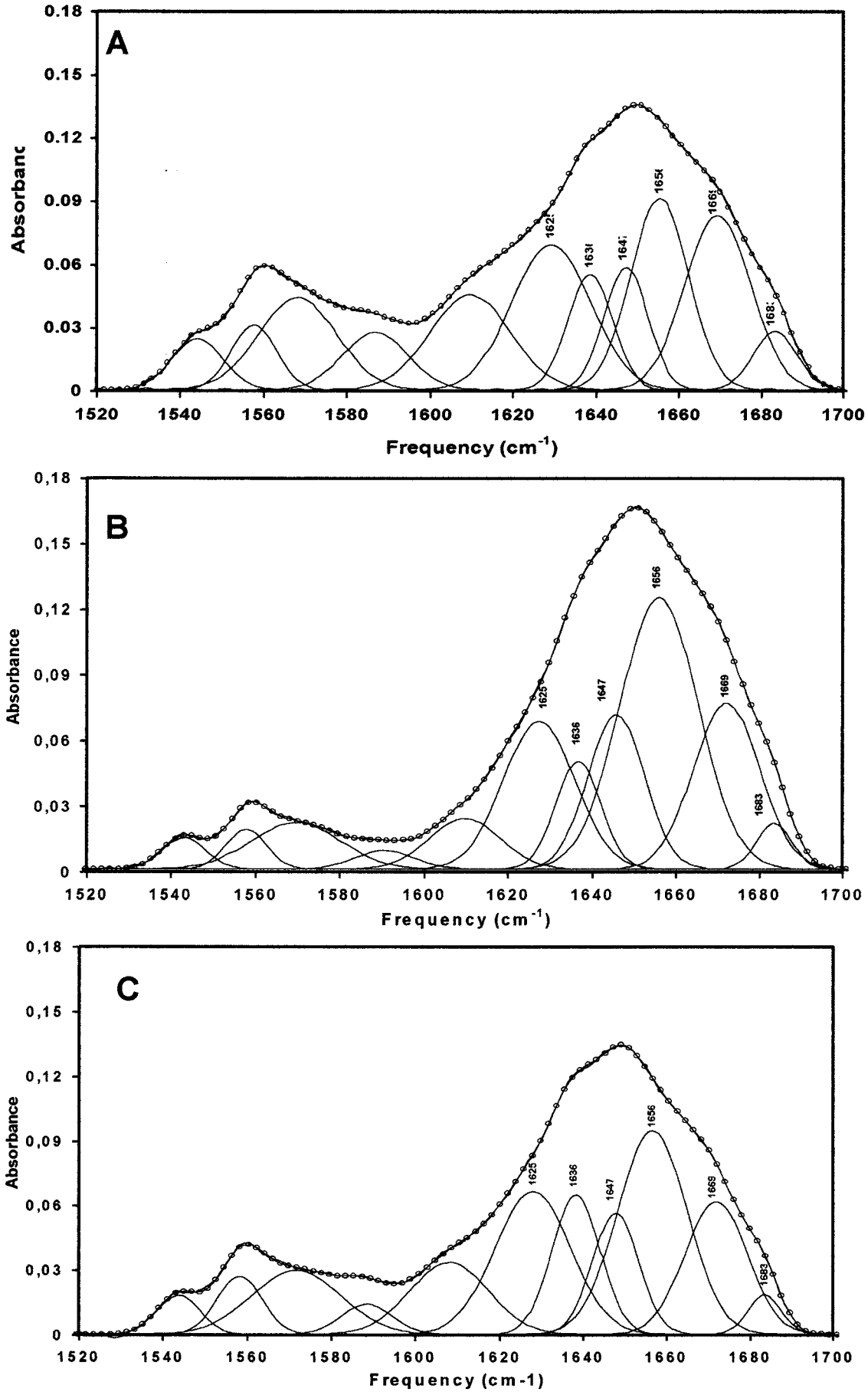

FIGURE 4: Amide I and amide II bands of the FTIR spectra of human prosomatostatin peptide analogues. The measured (—) and curve-fitting (—○—) spectra of peptides Som(Arg^{-15}—Lys^{-1})-PAMAP (A), Som(Arg^{-15}—Lys^{-1})-PAMAA (B), and Som(Arg^{-15}—Lys^{-1})-AAMAP (C) in a 50% D_2O/TFE-d_2 mixture are shown with the component bands resulting from the analysis (see Materials and Methods). Measurements at 25 °C were performed for 10 mg/mL concentration of peptides.

Table 3: Frequency and Quantitative Contribution of Each Spectral Band Component to the Total Amide I Contour of Each Somatostatin Analogue[a]

	frequencies (cm^{-1})					
	1626	1636	1647	1656	1669	1683
Som(Arg^{-15}−Lys^{-1})-PAMAP	19.5	14.9	12.7	26.7	23.2	2.8
Som(Arg^{-15}−Lys^{-1})-PAMAA	18.1	8.3	15.0	36.7	19.0	2.7
Som(Arg^{-15}−Lys^{-1})-AAMAP	22.9	14.3	12.0	30.3	17.6	2.7

[a] The numbers represent the calculated percent of each component obtained by FTIR spectra recorded in 50% TFE/H_2O solution using curve-fitting procedures (*25*−*28*).

The broad amide I contour of each spectrum is composed of six bands at 1683, 1669, 1656, 1647, 1636, and 1626 cm^{-1}. On the basis of different studies of peptide chains in proteins and peptides (*25*−*28*), the assignment of these bands can be summarized as follows. The 1626 and 1636 cm^{-1} components are generally attributed to β-sheet structures (*26*, *37*, *38*), whereas the bands in the 1690−1670 cm^{-1} region contain contributions from both turns or bends and β-sheet structures (*39*−*41*). However, on the basis of FTIR studies of model polypeptides as well as of proteins with very high β-sheet contents (*38*, *42*−*44*), it can be deduced that the bands around 1683 and 1667 cm^{-1} are indicative of residues engaged in turns or bends as well as to α-type helical structures with distorted hydrogen bonding (*40*, *45*, *46*). The 1656 cm^{-1} band as the amide I components observed in the region 1658−1650 cm^{-1} arises generally from α-helices (*26*, *45*). The amide I band, located at 1647 cm^{-1}, is generally associated with nonordered conformations or conformations in which the backbone folding shows no apparent periodicity (*25*, *26*). The remaining bands, situated outside the amide I region, are due to specific vibrations of amino acid side chains (*47*−*49*).

Table 3 summarizes the contribution of each band to the total amide I contour determined by curve-fitting procedures (*25*−*28*). These data bring evidence for the presence of an helical structure in the wild-type and mutated S-28(1−12) peptide sequences. Furthermore, when Ala was substituted for Pro^{-5} or Pro^{-9}, the percentage of α-helix calculated for the unmutated peptide Som[Arg^{-20}−Lys^{-1}]-PAMAP (27%, 6%) was enhanced by 10% and 4% for peptides Som-[Arg^{-20}−Lys^{-1}]-PAMAA and Som[Arg^{-20}−Lys^{-1}]-AAMAP, respectively (Table 3).

These CD and FTIR results, in agreement with the data obtained by the AGADIR method, underline the respective role of each proline residue in both the stability and the precise location of the helical structure adopted by the Ala-Met-Ala tripeptide motif.

Functional Role(s) of the Somatostatin-28(1−*12) Domain.* As shown in Figure 5A, the sequence of the S-28(1−12) domain contains two proline residues arranged as a P-$(X)_3$-P motif in the human and anglerfish I precursors or as a PP doublet in the anglerfish prosomatostatin II. Although the human and anglerfish I precursors share a similar pattern (P-$(X)_3$-P), it was shown that in vivo anglerfish prosomatostatin I undergoes a single cleavage at the dibasic site (*50*−*52*). Similarly, the S-28 hormone was exclusively released from the anglerfish precursor II which as the human mutant [P^{-6},P^{-5}] (Figure 1B) contains the PP motif. We attempted to define the structural basis responsible for these differences. The secondary structure of the Som[Xaa^{-20}−Asn^{+5}] sequence

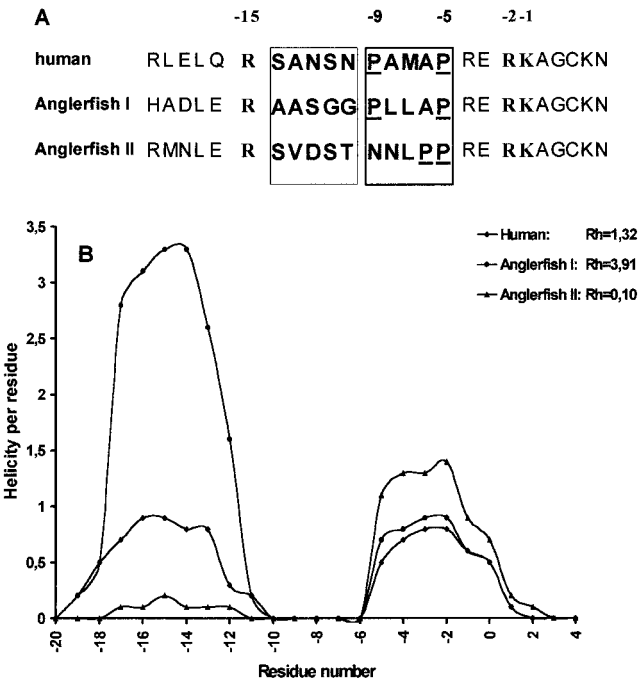

FIGURE 5: The somatostatin sequence [−20,+5] derived from different species. (A) Alignment of the human, anglerfish I, and anglerfish II sequences [−20,+5]. Proline residues are underlined. Open boxes indicate the motifs analyzed in each species. (B) Helicity per residue calculated for the Som(Xaa^{-20}−Asn^{-5}) sequence derived from the human and anglerfish I and II prosomatostatin. The values calculated for the parameter R_h are indicated in the insert.

Table 4: Functional Role of Each Motif of the Somatostatin-28(1−12) Segment[a]

modifications	human	anglerfish I	anglerfish II
P-$(Xaa)_3$-P	1.30	3.90	0.80
$(Xaa)_3$-P-P	0.40	7.20	0.10
Δ[P,P]	0.30	1.00	0.07
SANSN	1.30	2.60	0.90
AASGG	2.30	3.90	2.90
SVDST	0.45	0.30	0.10

[a] R_h = (total helicity values of segment [−20;−10])/(total helicity values of segment [−6;+5]).

was explored (Figure 5B). Analysis of data, obtained for all prosomatostatin species, revealed the following: (i) the main difference was observed in the helicity values per residues of fragment [−20;−10] which contains the monobasic site and (ii) the value of the parameter R_h (R_h = total helicity values of fragment [−20;-10]/total helicity values of fragment [−6;+5]) was 1.3, 3.9, and 0.1 for the human, anglerfish I, and anglerfish II precursors, respectively. On the basis of the data obtained for the human prosomatostatin mutants (Table 1 and Figure 2), these results argue in favor of the existence of functional relationships between the helicity ratio (R_h) and the proportions of S-14 and S-28 generated from each somatostatin precursor.

To test this hypothesis, we have investigated the secondary structure of Som[Xaa^{-20}−Asn^{+5}] peptides in which certain domains were either mutated or deleted. Results of these modifications (Table 4) allowed to deduce the following: (i) proline residues arranged as P^{-9}-$(X)_3$-P^{-5} or P^{6-}-P^{5-} motifs did not play any special role in the proportions of S-28 and S-14 molecules generated from anglerfish I and II

precursors and (ii) transfer of the [−14;−10] sequence from one species to another allows for each prosomatostatin species to mimic the other. Accordingly, these observations indicated that the proportions of S-28 and S-14 molecules generated from the anglerfish I and II prosomatostatins were not exclusively correlated with structure induced by the [−9;−5] sequence but were also related to the conformational organization of the S-28(1−12) molecule.

DISCUSSION

Earlier analysis of amino acid sequences around proteolytic cleavage sites of several biosynthetic precursors by secondary structure predictive methods (*31*) indicated that the dibasic residues constituting these cleavage sites are located in or immediately adjacent to regions with high β-turn formation propensity (*3*, *31*, *53*). Site-directed mutagenesis of prohormone cDNA coupled with spectroscopic and enzymatic studies of substrates reproducing the cleavage loci of various prohormones have shown that these β-turn structures situated in the vicinity of dibasic cleavage sites (*16*, *54*−*58*) constitute an essential feature for the processing of precursors (*14*, *36*, *54*, *57*).

Moreover, a series of observations deduced from different studies had also underlined the importance of certain residues other than the basic ones in specifying correct processing at the cleavage sites (*14*, *35*−*36*, *59*−*62*). Indeed, it was observed that the presence or absence of proline residues, in the vicinity of the dibasic cleavage site of the proOT/Np-(1−20) processing domain, induces the formation of different types of β-turn and also influences the basic side-chain orientation (*56*). Recently, these conformational features were shown to be important in dibasic cleavage by the prohormone convertase PC1/3 (*63*). In the case of the prosomatostatin processing, the two proline residues present in the S-28(1−12) sequence (see Figure 1A) were identified to be important in the production of equivalent amounts of the S-14 and S-28 molecules (*14*, *35*, *36*). When the sequence of the S-28(1−12) domain adopting a β-turn was replaced by nonhomologous peptide stretches capable of adopting an equivalent secondary structure, the proportions of S-14 and S-28 produced by the prosomatostatin mutants were different (*35*, *36*, *54*). Similar results were also obtained when the two prolines were replaced by glycine, which like proline increases the propensity for β-turns. Moreover, whereas replacement of Pro^{-5} or Pro^{-9} by alanine almost abolished selectively prosomatostatin processing at mono- and dibasic sites, respectively, the double mutation did not abolish cleavage at the monobasic one (*14*, *35*, *36*). In the present study the possible role of the P-A-M-A-P motif in particular, and the S-28(1−12) segment in general, was investigated by a combination of conformational analysis using AGADIR predictions and FTIR spectroscopy in relation with an evaluation of the processing efficiency of various prosomatostatin mutants in Neuro2A cells. The major conclusion of this report is that the P-A-M-A-P motif in particular and the S-28(1−12) sequence in general play a key role in prosomatostatin basic cleavage site exposure to processing enzymes.

The major emerging concept is that the Pro^{-9}-Ala-Met-Ala-Pro^{-5} sequence is a helical motif whose integrity is essential for prosomatostatin processing at both basic cleavage sites. This conclusion is supported by different observations. Indeed, substitution of Ala (which is the best α-helix-promoting amino acid residue) for Pro^{-5} or Pro^{-9} almost abolished processing of the precursor into S-14 and S-28, respectively (Table 1). These results, which suggest that a helical structure is involved in this phenomenon, are in good agreement with spectroscopic and predictive data obtained for synthetic peptides corresponding to the S-28(1−12) sequence bearing these mutations. Moreover, analysis of helicity profiles obtained by the AGADIR method indicated that these mutations favored the extension of an α-helix toward the dibasic site (from Asn^{-10} to Gly^{2} for the Ala^{-5} mutation) and the monobasic one (from Asn^{-12} to Pro^{-5} for the Ala^{-9} mutation), respectively. Altogether, these results demonstrate that the A-M-A sequence can be considered as the helical nucleation core of the P-A-M-A-P pattern. All mutants, and particularly those in which the A-M-A sequence or the proline residues were deleted (Δ[AMA] and Δ[PP] mutants, respectively), supported this conclusion since an increase of helicity propensity was in general correlated with the decrease of the cleavage at either the dibasic or the monobasic site.

Although mutation of proline residues almost abolished the cleavage at both basic sites, the absence of a proline residue at position −5 highly affected the processing of human prosomatostatin. Indeed, for the mutants in which Pro^{-5} or Pro^{-9} and Pro^{-5} were either mutated ([A^{-5}] and [A^{-9},A^{-5}] mutants), deleted (Δ[PP] mutant), or shifted ([P^{-9},P^{-6}] mutant), their processing efficiencies and the proportions of both the S-14 and S-28 molecules were low (Table 1). Similar effects have been already observed for other prosomatostatin mutants in which Gly was substituted for Pro^{-5} or Pro^{-9} or the original β-turn sequence was replaced by others lacking proline residues (*36*). This emphasizes the importance of Pro^{-5} since either its mutation or deletion favored the following: (i) the propagation of the helicity of the Ala-Met-Ala sequence toward the dibasic cleavage site and (ii) the amplification of this helical structure by the presence of residues Asn and Pro which were shown to have high specific preferences for the N-cap and N-cap + 1 of helices (*33*, *64*), respectively (i.e., Asn^{-12} for the [A^{-9},A^{-5}] and Δ[PP] mutants; Asn^{-10} and Pro^{-9} for the [A^{-5}] mutant). Accordingly, this explains both the differences observed in the percentages of helicity obtained for Som-[Arg^{-20}−Lys^{-1}]-PAMAA (37%, 6%) and Som[Arg^{-20}−Lys^{-1}]-AAMAP (31%, 6%) peptides and the high values of helicity predicted for the preceding mutants by the AGADIR method. Therefore, since mutation or shift of Pro^{-9} did not decrease the processing efficiency of the corresponding mutants (see Table 1), these observations indicate that Pro^{-5}, through the pattern P-A-M-A-P, plays an important role in the correct folding of the prosomatostatin processing domain. It is noteworthy that this particular amino acid residue is highly conserved in the primary sequence of prosomatostatin precursors from various species (*65*).

Although the present data underline the contribution of the P-A-M-A-P pattern to human prosomatostatin processing a question arises in the case of anglerfish islets where the mature S-14 and S-28 peptides are derived from two distinct precursors, anglerfish prosomatostatins I and II, respectively (*50*−*52*). Analysis of the Som[Xaa^{-20}−Asn^{+5}] sequence by the AGADIR method indicates that the source of this

difference resides in the peptide fragment [−20;−10] which contains the monobasic site (Figure 4A). This implies that other domain(s) participate also in the processing of those prohormone molecules. Such an interpretation is consistent with the following observations. First, deletion of the entire PAMAP motif did not abolish the cleavage of human prosomatostatin but rather increased the value of the S-28/S-14 ratio (see Table 1). Second, whereas modifications of the PAMAP pattern modulate the processing of human prosomatostatin, the data obtained for the anglerfish precursors indicated that the proline residues arranged as P-$(X)_3$-P or $(X)_3$-P-P motif could never modify their processing (i.e., the S-14 and S-28 hormones are exclusively released in vivo from anglerfish precursors I and II, respectively). Finally, exchange of the peptide fragment [−14;−10] between these precursors allowed each species to mimic in general the other. In light of these results, it could be concluded that the structural features involved in the processing specificity of prosomatostatin precursors reside necessarily in the S-28-(1−12) segment and its particular folding.

In conclusion, given the fact that the amino-terminal domain of prosomatostatin was suggested as a molecular signal for targetting the precursor in the intracellular secretory pathway *(66−69)*, the present report now documented for the first time the conformational contribution of the S-28-(1−12) connecting peptide in proteolytic processing of these prohormones. This function is most evident in the case of human prosomatostatin which appeared as a complex system. It shows the role of S-28(1−12) in directing cleavage at both basic sites via the P-A-M-A-P motif which contributes in maintaining an adequate conformation recognized by the specific prohormone convertase(s) to generate the normal S-28/S-14 ratio.

ACKNOWLEDGMENT

We thank Professor B. Alpert and Dr. S. Fermandjian for their help with FTIR and CD spectroscopy measurements and analysis.

REFERENCES

1. Seidah, N., Mbikay, M., Marcinkiewicz, M., and Chrétien, M. (1998) in *Proteolytic and Cellular Mechanisms in Prohormone Processing* (Hook, V., Ed.) pp 49−76, R. G. Landes Co., Georgetown, TX.
2. Zhou, A., Webb, G., Zhu, X., and Steiner, D. (1999) *J. Biol. Chem. 274*, 20745−20748.
3. Rholam, M., Nicolas, P., and Cohen, P. (1986) *FEBS Lett. 207*, 1−6.
4. Fuller, R., Sterne, R., and Thorner, J. (1988) *Annu. Rev. Physiol. 50*, 345.
5. Roebroek, A., Schalken, J., Leunissen, J., Onekink, C., Bloemers, H., and Van de Ven, W. (1986) *EMBO J. 5*, 2197.
6. Seidah, N., and Chrétien, M. (1994) *Methods Enzymol. 244*, 175−188.
7. Steiner, D. (1998) *Curr. Opin. Chem. Biol. 2*, 31−39.
8. Seidah, N., Chrétien, M., and Day, R. (1994) *Biochimie 76*, 197−209.
9. Seidah, N., Hamelin, J., Marmarbachi, M., Dong, W., Tadros, H., Mbikay, M., Chrétien, M., and Day, R. (1996) *Proc. Natl. Acad. Sci. U.S.A. 93*, 3388−3393.
10. Hook, V., Schiller, M., and Azaryan, A. (1996) *Arch. Biochem. Biophys. 328*, 107−114.
11. Pierotti, A., Prat, A., Chesneau, V., Gaudoux, F., Leseney, A. M., Foulon, T., and Cohen, P. (1994) *Proc. Natl. Acad. Sci. U.S.A. 91*, 6078−6082.
12. Plevrakis, I., Creminon, Ch., Clamagirand, Ch., Brakch, N., Rholam, M., and Cohen, P. (1989) *Biochemistry 28*, 2705−2710.
13. Rholam, M., Clamagirand, Ch., and Cohen, P. (1997) in *Handbook of Proteolytic Enzymes* (Barrett, A. J., Rawlings, N. D., and Wooesner, J. F., Eds.) Vol. 540, pp 1544−1546, Academic Press, London.
14. Gomez, S., Boileau, G., Zollinger, L., Nault, C., Rholam, M., and Cohen, P. (1989) *EMBO J. 8*, 2911−2916.
15. Brakch, N., Boussetta, H., Rholam, M., and Cohen, P. (1989) *J. Biol. Chem. 264*, 15912−15916.
16. Rholam, M., Cohen, P., Brakch, N., Paolillo, L., Scatturin, A., and Di Bello, C. (1990) *Biochem. Biophys. Res. Commun. 168*, 1066−1073.
17. Brakch, N., Galanopoulou, A., Patel, Y., Boileau, G., and Seidah, N. (1995) *FEBS Lett. 362*, 143−146.
18. Bourdais, J., Pierotti, A., Boussetta, H., Barre, N., Devilliers, G., and Cohen, P. (1991) *J. Biol. Chem. 266*, 23386−23391.
19. Munoz, V., and Serrano, L. (1997) *Biopolymers 41*, 495−509.
20. Tabor, S., and Richardson, C. (1987) *Proc. Natl. Acad. Sci. U.S.A. 84*, 4767−4771.
21. Noel, G., Zollinger, L., Laliberte, F., Rassart, E., Crine, P., and Boileau, G. (1989) *J. Neurochem. 52*, 1050−1057.
22. Brakch, N., Cohen, P., and Boileau, G. (1994) *Biochem. Biophys. Res. Commun. 205*, 221−229.
23. Venyaminov, S., and Yang, J. (1996) *Circular Dichroism and the Conformational Analysis of Biomolecules* (Fasman, G., Ed.) Plenum Press, New York and London.
24. Moriarty, D., and Raleigh, D. (1999) *Biochemistry 38*, 1811−1818.
25. Surewicz, W., Mantsch, H., and Chapman, D. (1993) *Biochemistry 32*, 389−394.
26. Byler D., and Susi, H. (1986) *Biopolymers 3*, 469−487.
27. Bandekar, J. (1992)*Biochim. Biophys. Acta 1120*, 123−143.
28. Jackson, M., and Mantsch, H. (1995) *Crit. Rev. Biochem. Mol. Biol. 30*, 35−120.
29. Kartha, G., Ashida, T., and Kakuda, M. (1974) *Acta Crystallogr., Sect. B: Struct. Sci. 30*, 6541−6548.
30. Von Heijne, G. (1991) *J. Mol. Biol. 218*, 418−503.
31. Rholam, M., and Cohen, P. (1994) in *Neuroprotocols: A Companion to Methods in Neuroscience* (Beinfeld, M. C., Ed.) Vol. 8, pp 130−143, Academic Press, New York.
32. Vanhoof, G., Goossens, F., De Meester, I., Hendriks, D., and Scharpe, S. (1995) *FASEB J. 8*, 736−744.
33. Richardson, J., and Richardson, D. (1988) *Science 240*, 1648−1652.
34. MacArthur, M., and Thornton, J. (1991) *J. Mol. Biol. 218*, 397−412.
35. Brakch, N., Rholam, M., Nault, C., Boileau, G., and Cohen, P. (1991) *FEBS Lett. 282*, 363−367.
36. Brakch, N., Rholam, M., Boussetta, H., and Cohen, P. (1993) *Biochemistry 32*, 4925−4930.
37. Dong, A., Huang, P., and Caughey, W. (1990) *Biochemistry 29*, 3303−3308.
38. Kalnin, N., Baikalov, I., and Venyaminov, S. (1990) *Biopolymers 30*, 1273−1280.
39. Halverson, K., Fraser, P., Kirschner, D., and Lansbury, P. (1990) *Biochemistry 29*, 2639−2644.
40. Prestrelski, S., Byler, D., and Liebman, M. (1991) *Biochemistry 30*, 133−143.
41. Kennedy, D., Crisma, M., Toniolo, C., and Chapman, D. (1991) *Biochemistry 30*, 6541−6548.
42. Arrondo, J., Young, N., and Mantsch, H. (1988) *Biochim. Biophys. Acta 952*, 261−268.
43. Casal, H., Kohler, U., and Mantsch, H. (1988) *Biochim. Biophys. Acta 957*, 11−20.
44. Dousseau, F., and Pézolet, M. (1990) *Biochemistry 29*, 8771−8779.
45. Krimm, S., and Bandekar, J. (1986) *Adv. Protein Chem. 38*, 181−364.

46. Urbanova, M., Dukor, R., Pancoska, P., Gupta, V., and Keiderling, T. (1991) *Biochemistry 30*, 10479−10485.
47. Holloway, P., and Mantsch, H. (1989) *Biochemistry 28*, 931−935.
48. Chirgadze, Y., Fedorov, O., and Trushina, N. (1975) *Biopolymers 14*, 679−694.
49. Venyaminov, S., and Kalnin, N. (1990) *Biopolymers 30*, 1243−1257.
50. Spiess, J., and Noe, B. (1985) *Proc. Natl. Acad. Sci. U.S.A. 82*, 277−281.
51. Noe, B., Andrews, P., Dixon, J., and Spiess, J. (1986) *J. Cell Biol. 103*, 1205−1211.
52. Morel, A., Kuks, P., Bourdais, J., and Cohen, P. (1988) *Biochem. Biophys. Res. Commun. 151*, 347−354.
53. Bek, E., and Berry, R. (1990) *Biochemistry 29*, 178−183.
54. Rholam, M., and Cohen, P. (1997) *Anal. Chim. Acta 352*, 155−178.
55. Weiss, M., Frank, B., Khait, I., Pekar, A., Heiney, R., Shoelson, S., and Neuringer, L. (1990) *Biochemistry 29*, 8389−8401.
56. Paolillo, L., Simonetti, M., Brakch, N., D'Auria, G., Saviano, M., Dettin, M., Rholam, M., Scatturin, A., Di Bello, C., and Cohen, P. (1992) *EMBO J. 11*, 2399−2405.
57. Rayne, R., and O'Shea, M. (1993) *Eur. J. Biochem. 217*, 905−911.
58. Falcigno, L., Paolillo, L., D'Auria, G., Saviano, M., Simonetti, M., and Di Bello, C. (1996) *Biopolymers 39*, 837−848.
59. Oda, K., Misumi, Y., Sohda, M., Takami, N., Sakaki, Y., and Ikehara, Y. (1991) *Biochem. Biophys. Res. Commun. 175*, 690−696.
60. Nagaham, M., Najayama, K., and Murakami, K. (1991) *Eur. J. Biochem. 197*, 135−140.
61. Mark, M., Lokker, N., Zioncheck, T., Luis, E., and Godowski, P. (1992) *J. Biol. Chem. 267*, 26166−26171.
62. Bristol, J., Furie, B., and Furie, B. (1993) *J. Biol. Chem. 268*, 7577−7584.
63. Brakch, N., Rholam, M., Simonetti, M., and Cohen, P. (2000) *Eur. J. Biochem. 267*, 1626−1633.
64. Chakrabarthy, A., Doig, A., and Baldwin, R. (1993) *Proc. Natl. Acad. Sci. U.S.A. 90*, 11332−11336.
65. Argos, P., Taylor, W., Minth, C., and Dixon, J. (1983) *J. Biol. Chem. 255*, 8788−8793.
66. Sevarino, K., Stork, Ph., Ventimiglia, G., and Goodman, R. (1989) *Cell 57*, 11−19.
67. Stoller, T., and Shields, D. (1989) *J. Cell Biol. 108*, 1647−1655.
68. Mitra, J., Tang, X., Almo, S., and Shields, D. (1998) *Biochem. J. 334*, 275−282.
69. Mouchantaf, R., Kumar, U., Sulea, T., and Patel, Y. (2001) *J. Biol. Chem. 255*, 8788−8793.

BI011928M